Monolayer Transition Metal Dichalcogenide Channel-Based Tunnel Transistor

Ram Krishna Ghosh and Santanu Mahapatra, *Senior Member, IEEE*

***Abstract*—We investigate the gate controlled direct band-to-band tunneling (BTBT) current in monolayer transition-metal dichalcogenide (MX_2) channel-based tunnel field effect transistor (TFET). Five MX_2 materials (MoS_2, $MoSe_2$, $MoTe_2$, WS_2, WSe_2) in their 2-D sheet forms are considered for this purpose. We first study the real and imaginary band structure of those MX_2 materials by density-functional theory (DFT), which is then used to evaluate the gate-controlled current under the Wentzel-Kramers-Brillouin (WKB) approximation. It is shown that all five MX_2 support direct BTBT in their monolayer sheet forms and offer an average ON current and subthreshold slope of 150 μA/μm (at $V_d = 0.1V$) and 4 mV/dec, respectively. Furthermore, we also demonstrate the strain effect on the complex band structures and the performances of MX_2 based TFETs. It is observed that a certain tensile strain becomes favorable for the improvement of ON-current performances.**

***Index Terms*—Tunnel field effect transistor, 2-D crystal, atomistic simulation, complex band structure, band-to-band tunneling.**

I. Introduction

THE TUNNEL field effect transistors (TFETs) with gate controlled band-to-band tunneling (BTBT) have emerged as a thrust area of research for low-standby power (LSTP) application due to its sub-60 mV/dec subthreshold swings (SS) and very high I_{ON}-I_{OFF} ratio [1], [2]. However, poor SS and low ON-current have been seen in all conventional Silicon TFETs due to the large indirect energy band gap ($\sim$1.12 eV). As a result, there has been an extensive investigation on the alternative materials for TFET applications [1]–[3] which do not require phonon assistance in the tunneling process. In order to replace Si, atomically thin layered materials have found great significance as alternate MOSFET channel materials due to their planar structure, excellent electrostatic integrity and mechanical flexibility. Recently, layered transition-metal dichalcogenide materials (MX_2) (Fig. 1), especially MoS_2, have received much attention for their application in nano-scale electronic devices as an alternative to Graphene [4]–[6].

Manuscript received June 17, 2013; revised August 28, 2013 and October 10, 2013; accepted November 21, 2013. Date of publication November 26, 2013; date of current version January 28, 2014. This work was supported by the Department of Science and Technology, Government of India, under Grant SR/S3/EECE/0151/2012. The review of this paper was arranged by Editor K. Shenai.

The authors are with the Nano-Scale Device Research Laboratory, Department of Electronic Systems Engineering, Indian Institute of Science, Bangalore 560012, India (e-mail: ramki.phys@gmail.com; santanu@cedt.iisc.ernet.in).

Color versions of one or more of the figures in this paper are available online at http://ieeexplore.ieee.org.

Digital Object Identifier 10.1109/JEDS.2013.2292799

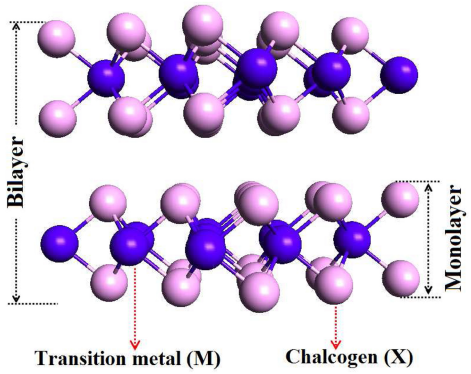

Fig. 1. Side view of the layer structure of 2D-hexagonal MX_2 crystals. Monolayer consists of a sandwich of three hexagonally packed atomic layers, X-M-X, where within two X layers, the M atoms in the intermediate layer are bonded with the X atoms through ionic-covalent interactions in a trigonal prismatic arrangement.

The bulk MX_2 crystals, which are composed of stacked layers, have indirect band gaps whereas these band gaps become direct in monolayer MX_2 form at the K point along the Γ-M-K-Γ path of the Brillouin zone [7]–[16] and thus may become a potential material for TFET applications.

In this paper, we first explore the BTBT in five monolayer MX_2 sheets (MoS_2, $MoSe_2$, $MoTe_2$, WS_2, and WSe_2) by considering the complex dispersion relationship within the band gap region. These complex band structure calculations have been evaluated by using Atomistix ToolKit (ATK) which uses DFT-LDA method [17]. Finally, computing the least action integral from the complex band structure and considering the analytical Poisson solution we compute the drain current of a symmetric double gate (DG) TFET and compare the performances of different MX_2 materials. Further, the impact of isotropic biaxial (ε^{bi}) and uniaxial (ε^{uni}) strains on the complex band structures and the performances of MX_2 based TFETs have also been investigated.

II. Approach, Results and Discussions

A. Study of Complex Band Structure

The band structure calculations of geometrically optimized MX_2 have been evaluated by using the ATK simulation package [17]. Our band structure computations are based on the self consistent density-functional theory (DFT). The exchange correlation energies are treated within local density approximation (LDA) combining with Perdew and Zunger correlation functional and double zeta polarized basis set.

TABLE I
ELECTRONIC, DIELECTRIC AND PHYSICAL PROPERTIES OF MX_2

MX_2	E_g (eV)		ξ_I (V nm^{-1})	$\varepsilon_s(\varepsilon_0)$		$c/2$ (nm)	λ (nm)
	Cal.[i]	Exp.		$\varepsilon_s^{\parallel}$	$\varepsilon_s^{\perp}$		
MoS_2	1.81	1.89[ii]	1.02	8.29	3.92[iii]	0.62	0.38
$MoSe_2$	1.58	1.55[iv]	0.85	9.05	6.07	0.65	0.45
$MoTe_2$	1.12	1.15[v]	0.81	33.70	16.10	0.70	0.72
WS_2	1.90	2.05[vi]	1.25	7.95	5.14	0.62	0.42
WSe_2	1.60	1.49[vii]	0.96	7.25	5.16	0.65	0.43

E_g is the energy band gap of monolayer MX_2. i = comparable with [7]–[9]. ii, iv-vii: [10]– [14].
ξ_I is the "least action integral" and has been calculated according to Eq. (1).
ε_s is the static dielectric constant of bulk, Re[$\varepsilon(\omega = 0)$], where "$\parallel$" and "$\perp$" represents the lateral and perpendicular directions of the material, respectively. iii = comparable with [6].
$c/2$ (c; bulk lattice constant) is the monolayer thickness, obtained from ab-initio structure optimization, which is close to the experimental value [4], [10], [15]– [16].
λ is natural length scale and has been calculated from Eq. (3) by considering 2 nm thick HfO_2 ($\varepsilon_{ox} = 25\varepsilon_0$) as a gate dielectric.

The tolerance parameter was 10^{-5} with maximum steps of 200, and a Pulay mixer algorithm [18] was used as the iteration control parameter. In addition, the k-point sampling of $27\times27\times1$ grid was used with a mesh cut-off energy of 10 Hartree. In case of monolayer MX_2 sheets we used a supercell with a 15$\mathring{A}$ vacuum region along the c axis (keeping the lattice parameters a and b same as bulk) so that it effectively behaves as an isolated 2D layer. Band gap values obtained from DFT are also in good agreement with existing experimental results as shown in Table I.

The static dielectric constant, Re[$\varepsilon(\omega = 0)$], [Table I] is computed by using DFT-LDA and double zeta double polarized basis set along with the k-point sampling of $15\times15\times15$ grid with a mesh cut-off energy of 75 Hartree. The Kubo-Greenwood formula has been used to calculate the susceptibility tensor ($\chi(\omega)$) [19], [20] which is related to the dielectric constant as $\varepsilon(\omega) = (1 + \chi(\omega))\,\varepsilon_0$, where ε_0 is the vacuum permittivity. In Table I, the bulk values of the dielectric constants are presented since the monolayer values are nearly same as those of the bulk. For example, the $\varepsilon_s^{\perp}$ of bulk MoS_2 is $3.92\varepsilon_0$ whereas it is $3.86\varepsilon_0$ for a monolayer sheet. So, for our device applications we approximated the monolayer dielectric values with the bulk values.

Recently, the complex band theory was successfully applied in the modeling of tunneling devices [21], [23], [24] for a deeper understanding of band-to-band tunneling (BTBT) phenomenon. Physically, during this BTBT process, when a carrier tunnels through a band gap region, it transits in an evanescent mode and its wave vector becomes imaginary within this forbidden gap. In case of direct band gap semiconductors, when the complex band that starts from the top of valence band '*wraps*' itself to the bottom of the conduction band, constituting one continuous band then only the direct BTBT can take place. However, if the band that starts from the valence band edge '*crosses*' with the band starting from the conduction band edge then the tunneling process requires phonon to ensure the momentum conservation [23] which reduces the transmission rate quite significantly [23], [25]. It

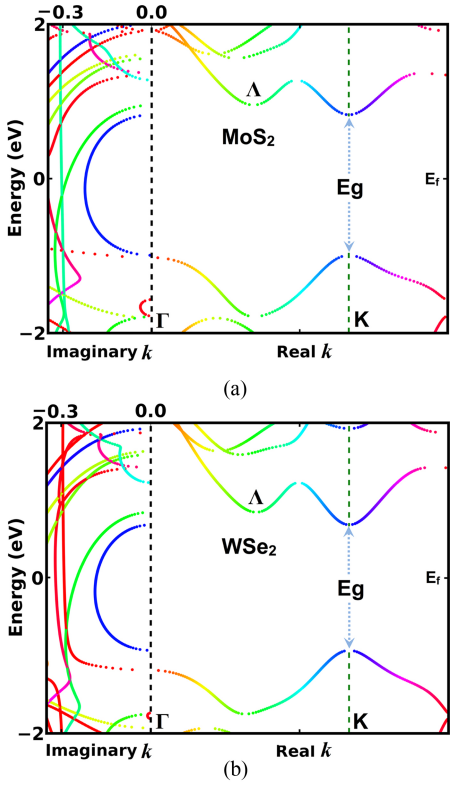

Fig. 2. Complex and real bands of monolayer MX_2 sheets. Here, we have shown the band structures of MoS_2 and WSe_2 only, as remains have same nature. The color-coding of the k-values applies to both real and imaginary parts of the band structure to make it easier to realize where the complex bands are attached to the real ones. E_g and E_f are band gap and the Fermi level respectively.

should also be noted that the inter-band tunneling probability (T_{BTBT}) depends on the minimum area that is enclosed by the complex band which connects the valence band edge to conduction band edge [21]–[24], [26]. Fig. 2 shows the complex bands within the band gap region of monolayer MX_2 monolayers. For clarity, only a few bands are shown here. It appears that, for all monolayer MX_2 monolayers, the complex band is characterized by a continuous band that connects the highest valence subband to the lowest conduction subband allowing for direct tunneling.

Now, using the Wentzel-Kramers-Brillouin (WKB) approximation the direct tunneling probability for the BTBT process can be approximated as [21], [27]

$$T_{BTBT} = \exp\left\{-\frac{2}{q\xi}\int_0^{E_g} k\,(E)\,dE\right\} \equiv \exp\left\{-\frac{\xi_I}{\xi}\right\} \qquad (1)$$

where q is the electronic charge, ξ the electric field; $E = 0$ the valence band edge, $E = E_g$ the conduction band edge, $k(E)$ the magnitude of the imaginary wave vector with "least action for tunneling" within the forbidden gap, and $\xi_I = \frac{2}{q}(\int_0^{E_g} k(E)dE)$ is basically the "*least action integral*" which is an intrinsic property of the material.

As a result, in any applied electric field, controlled by a third terminal (the gate) in TFET applications, T_{BTBT} can be figured out instantly when ξ_I is enumerated. Since monolayer $MoTe_2$

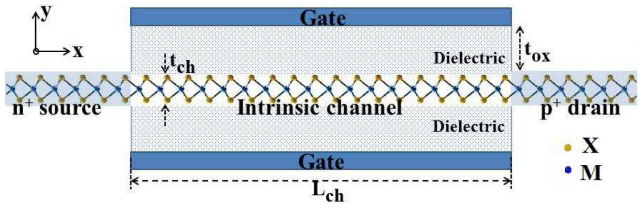

Fig. 3. Schematic cross section of a monolayer MX_2 based double gate TFET with n^+ source, p^+ drain and intrinsic channel.

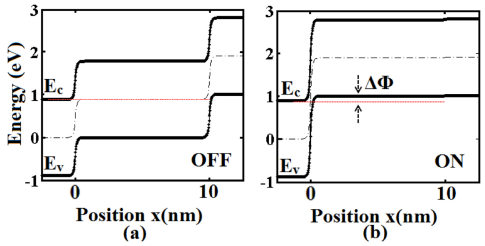

Fig. 4. Energy band diagrams for a symmetric n^+-i-p^+ DG TFET having monolayer MoS_2 sheet as a channel material in (a) the OFF-state and (b) the ON-state respectively.

sheet has lowest direct band gap than others, it provides the lowest ξ_I value [Table I]. It is recently noticed that the presence of spin orbit coupling can split the valence band maximum at the K-point [28]. However, the curvatures of the conduction band minima and valence band maxima remain same. It is also observed that the band gap remains nearly same for with or without spin orbit coupling. Therefore, the inclusion of spin-orbit coupling does not affect the tunnelling effective mass as well as the band gap which are responsible to find ξ_I to calculate the band to band tunnelling probability.

B. Calculation of TFET Drain Current

Now, we investigate the performance of the symmetric DG TFET with these materials as channel materials (Fig. 3) with a thickness of t_{ch} ($= n \times \frac{c}{2}$; n is the number of layers) and an oxide thickness of t_{ox}. The source region is heavily n^+ doped and drain is heavily p^+ doped, while the channel of length L_{ch} is intrinsic. We also consider that, in an electrostatically well-designed device, the Fermi level is at the conduction band edge (E_c) at the n^+ source and at the valence band edge (E_v) at the p^+ drain whereas it is at the mid-gap of the intrinsic channel at thermal equilibrium. To demonstrate the surface potential profile (Ψ_s) in this DG TFET, here we use an analytical model which shows that the electrostatic of such TFET can be described by a modified 1-D Poisson equation [29]

$$\frac{d^2\Psi_s}{dx^2} - \frac{\Psi_s - V_g + V_{bi}}{\lambda^2} = 0 \tag{2}$$

where x is the direction along the channel, V_g and V_{bi} ($\approx \frac{E_g}{2q}$) are the gate and built-in potentials respectively, and λ is the natural length scale of the potential variation and is given by

$$\lambda = \sqrt{\frac{\varepsilon_{ch}}{2\varepsilon_{ox}}\left(1 + \frac{\varepsilon_{ox}}{4\varepsilon_{ch}}\frac{t_{ch}}{t_{ox}}\right)t_{ch}t_{ox}} \tag{3}$$

Here, ε_{ch} ($= \varepsilon_s^{\perp}$) and ε_{ox} are the channel and oxide dielectric constants respectively. Applying the following boundary conditions (i) zero electric field at $x = \pm\infty$ and (ii) continuous

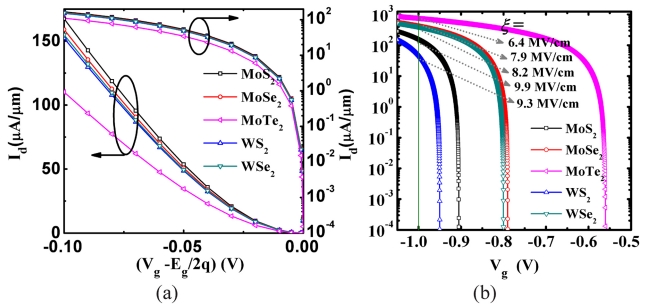

Fig. 5. Direct tunneling current variation with (a) $(V_g - \frac{E_g}{2q})$ and (b) V_g in a symmetric n^+-i-p^+ DG TFET having monolayer MX_2 sheets as channel materials at $V_d = 0.1$ V and $T = 300K$.

electric field and potential at the source-channel and drain-channel junction, and (iii) $L_{ch} \gg \lambda$, (2) can be solved analytically and leading to a solution of the form $\Psi_s \propto \exp(-\frac{x}{\lambda})$. The electric field calculated from the surface potential profile can then be expressed as $\xi \propto \frac{1}{\lambda}(\frac{E_g}{2q} - V_g)e^{-\frac{x}{\lambda}}$. Now, from (3) it is also seen that λ is a function of t_{ch} and this solution reflects that the source-channel junction will become very thin in case of an atomically thin planar structure (see Table I). Being a function of t_{ox} and ε_{ox}, it can also be seen that λ decreases as t_{ox} decreases and the gate dielectric constant increases. If we compute the λ of MoS_2 by considering 2 nm thick HfO_2 ($\varepsilon_{ox} = 25\varepsilon_0$) as a gate dielectric then it gives only 0.38 nm whereas 5 nm thick ultrathin-body Si or InAs provides a λ of 2.35 or 2.48 nm. Thus these MX_2 provides 6–7 times smaller value of λ than the conventional ultrathin materials. In case of low band gap materials (e.g. III–V materials) the ξ_I is significantly low, however as the tunneling probability is controlled by the product $\lambda \times \xi_I$ thus higher λ reduces the tunneling probability. So the use of high-κ oxide and atomically thin planer channel materials will improve the device performance significantly [30]. In this context, it should be noted that the change in Ψ_s at the middle of the channel should not depend on drain voltage for proper BTBT process in TFET operation. This can be achieved if $L_{ch} \gg \lambda$ and the scaling of the device is in the quantum capacitance limit (QCL) that can also be achieved in monlayer 2-D MX_2 sheets due to their low DOS value [6], [9], [31].

Considering HfO_2 as a dielectric ($\varepsilon_{ox} = 25\varepsilon_0$, $t_{ox} = 2$ nm) and monolayer MoS_2 sheet as a channel ($L_{ch} = 10$ nm), the computed band diagrams for a symmetric n^+-i-p^+ DG TFET are shown in Fig. 4(a) for the OFF-state at $V_g = 0$ and in Fig. 4(b) for the ON-state at $V_g = -1.0$ V with a supply voltage (V_d) of 0.1 V. It can be seen from Fig. 4(b) that under this condition, the reverse-bias V_g opens an energy window, $\Delta\Phi$, through which the effective tunneling current flows and this $\Delta\Phi$ can be derived as $(qV_g - \frac{E_g}{2})$. It should also be noted that this $\Delta\Phi$ is derived here for relatively small V_g, so that the effective electric field do not change appreciably from its equilibrium value. Under these circumstances, the BTBT tunneling current can be then written in the form [22]

$$I_{BTBT} = \frac{g_s g_v q}{h}\int_0^{\Delta\Phi} T_{BTBT}\left\{f_i(E) - f_f(E)\right\}dE \tag{4}$$

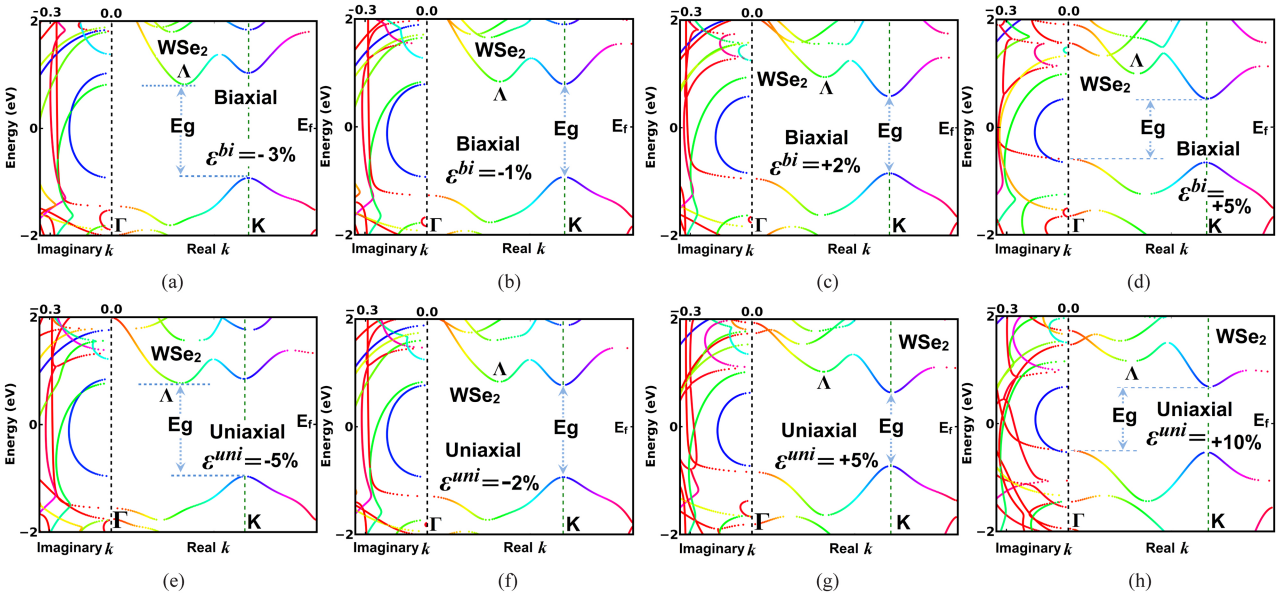

Fig. 6. Effect of various biaxial ((a)–(d)) and uniaxial ((e)–(f)) strains on the complex and real bands of monolayer WSe_2 sheet. '+' and '−' represent the tensile and compressive strain respectively. The color-coding of the k-values indicates where the complex bands are attached to the real ones.

in which h is the Planck's constant; $g_s(=2)$ and g_v $(=2)$ are the spin and valley degeneracies [7]; $f_i(E)$ and $f_f(E)$ are the Fermi functions of the initial and final states from and to which the tunneling occurs, respectively. Using (1) and (4), taking $\Delta\Phi$ and ξ across the source-channel junction (x=0) from the band diagram calculations for different channel materials, the drain-current (I_d) at room temperature can be then calculated as a function of the V_g. It can be seen from Fig. 4(b) that, to open an energy window for tunneling, a reverse-bias $V_g = \frac{E_g}{2q}$ should require and that will be different for different channel materials. So, to compare the On-current performances, in Fig. 5 we have presented the variation of the direct BTBT current per micron width as a function of $(V_g - \frac{E_g}{2q})$ for monolayer MX_2 sheets at a supply voltage $V_d = 0.1$ V. It appears from Fig. 5 that, in all cases the drive tunneling currents show the same kind of variations, however, MoS_2 has the best performance compared to others. Although it has relatively higher ξ_I value, a comparatively lower ε_{ch} and t_{ch} provides much lower λ (see Table I) and consequently it delivers better ON-performance. On the other hand, $MoTe_2$ has much lower band gap so the effective tunneling will start in very low V_g for this material. Thus, if we see the variation as a function of V_g only, then $MoTe_2$ sheet (lowest band gap) will provide highest performance for a particular V_g (Fig. 5(b)) which is consistent with the results in [32]. While in comparison to the conventional Si TFET which shows only 0.4μA/μm for the comparable $V_d = 0.1$ and $V_g - V_{th} = 0.1$ V (V_{th}; the threshold voltage) [33], MX_2 sheets provide much higher ON-currents. In case of Graphene nanoribbon (GNR), as investigated earlier by Q. Zhang et al. [34], it can be seen that the ON state current is 800 μA/μm for 5nm wide monolayer GNR ($E_g \sim 0.25$ eV). However, owing to much higher band gap, MX_2-TFET offers negligible OFF-current in comparison to GNR. Therefore, the atomically thin transition metal dichalcogenides have an advantage over Graphene nanoribbons whose band gap decreases very rapidly with the increase of ribbon width and becomes very small above 5nm. An average subthreshold slope less than 4 mV/dec (extracted from the I_d - V_g characteristics using the same method as in [30]), shows the immense potential of MX_2 based TFETs for realizing high performance LSTP devices.

C. Effect of Elastic Strain

Recently, strain dependent modulation of the transport properties of a channel material has successfully been employed in the CMOS technology to improve the carrier mobility and ON-current performances in the devices [35], [36]. Keeping that in mind, in the next part we have investigated the impact of strain on the performances of the MX_2 based TFETs. In our study, the strain is given by scaling the lattice constant of the MX_2 by an amount $\varepsilon = (a - a_0)/a_0$, where a_0 and a are the lattice constants of the unstrained and strained MX_2 sheet respectively.

Fig. 6 shows the effect of in-plane isotropic biaxial, ε^{bi} ($\varepsilon_{xx} = \varepsilon_{yy}$) and uniaxial ε^{uni} (ε_{xx}) strain on WSe_2 sheet. Previously, in the relaxed case we have seen that the band structure is direct in nature (Fig. 2), having both conduction band minima (E_c^{min}) and valence band maxima (E_v^{max}) at the K-point in the Brillouin zone; however, it appears from Fig. 6 that if we provide strain then the nature of WSe_2 band structure undergoes a direct to in indirect band gap transition. If we provide a strain of $\varepsilon^{bi} \simeq +3.75\%$ (or $\varepsilon^{uni} \simeq +9\%$) then it is seen that the E_v^{max} at the Γ point moves up than the K point and makes the band gap as an indirect one. On the other hand, with the application of $\varepsilon^{bi} \simeq -1.5\%$ (or $\varepsilon^{uni} \simeq -3.5\%$), the E_c^{min} at the Λ moves down than the K point and band gap becomes indirect (see Fig. 6). It is worth noting that as the energy difference of the E_v^{max} (or E_c^{min}) between Γ (or Λ) and K point is different for the various MX_2, therefore the direct to indirect transition attains at various tensile or compressive

TABLE II
STRAINS TO ATTAIN DIRECT TO INDIRECT BAND GAP TRANSITION OF VARIOUS MX_2

MX_2	ε^{bi} (%)		ε^{uni} (%)	
	Tensile	Compressive	Tensile	Compressive
MoS_2	+0.65	−1.25	+1.0	−1.0
$MoSe_2$	+3.6	−0.9	+8.0	−1.5
$MoTe_2$	+5.5	−1.0	+7.5	−2.0
WS_2	+0.5	−1.3	+1.05	−1.4
WSe_2	+3.75	−1.5	+9.0	−3.5

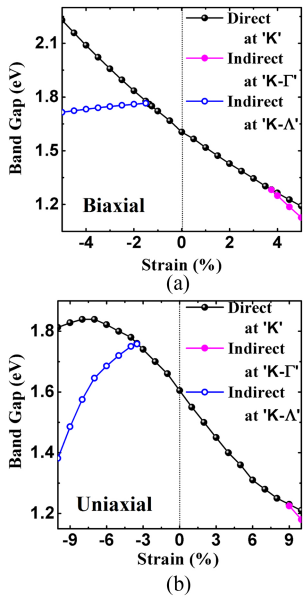

Fig. 7. The energy band gap variation of WSe_2 sheet under (a) isotropic biaxial and (b) uniaxial strains. The direct band gap is always measured at the K point of the Brillouin zone. The '$+ve$' and '$-ve$' side represent the tensile and compressive strain respectively.

strains for different MX_2 materials (see Table II). The nature of our computed band structure results are also in good agreement with the previous theoretical investigations [37], [38].

Moreover, it also appears from Fig. 7 that the band gap of WSe_2 (and other MX_2 also) changes significantly with the increase of both biaxial as well as uniaxial strain. With the increase of tensile strain, the direct band gap decreases for both ε^{bi} and ε^{uni} whereas it increases with the increase of compressive strain. However, this direct band gap again decreases slowly above $\varepsilon^{uni} = -7\%$. On the other hand, the indirect band gap decreases with the increase of both tensile and compressive strains after the direct to indirect transition. We can further see that the difference in indirect to direct band gap in the tensile zone is much less than the difference in the compressive zone.

Recently, it is also investigated that if the energy difference between the direct and indirect band gap is quite small then the transmission probability for direct band gap transitions dominates over the probability for indirect band gap transitions [26], [39]. Therefore, reducing the barrier height with the application of tensile strain will be an encouraging technique to increase the direct BTBT current in MX_2 based TFET applications.

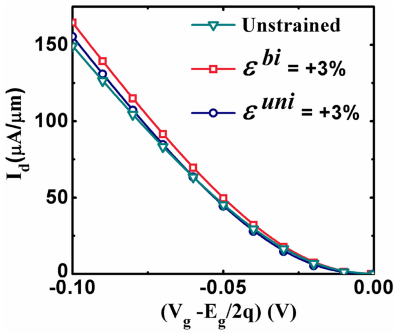

Fig. 8. Direct tunneling current variation with V_g in a symmetric DG TFET having monolayer WSe_2 sheet as channel materials at V_d = 0.1 V and $T = 300K$ for various strains.

In Fig. 8 we have shown the ON-current performances of WSe_2 sheet for various tensile strains by considering the same channel dielectric constant as the change in dielectric constant is negligibly small with strain (not shown here). It appears that the ON-current increases $\sim$ 13% (or $\sim$ 9%) with the application of ε^{bi} = +3% (or ε^{uni} = +3%). Therefore, under tensile strain condition, the ON-current performance increases well for same oxide dielectric, a trait beneficial for TFET application.

Finally, we wish to state that in this present case we did not contemplate the influence of phonon scattering and impurity scattering that should be considered to provide a more complete picture of a practical device model, which is well beyond the scope of this paper.

III. CONCLUSION

We have investigated the direct band-to-band tunneling current in transition-metal dichalcogenide channel based tunnel field effect transistor (TFET) by studying their complex band structures by DFT-LDA. It is observed that all the five MX_2 sheets support direct BTBT in their unstained forms. Further, it is investigated that the application of tensile strain can also favorable to increase the ON-current performances. Relatively higher tunneling current, much lower SS value and better gate controllability in MX_2 based TFETs indicate that these may become the promising channel materials for future TFET applications.

REFERENCES

[1] J. Appenzeller, Y. M. Lin, J. Knoch, and P. Avouris, "Band-to-band tunneling in carbon nanotube field-effect transistors," *Phys. Rev. Lett.*, vol. 93, no. 19, pp. 196805(1)–196805(4), Nov. 2004.
[2] A. M. Ionescu and H. Riel, "Tunnel field-effect transistors as energy-efficient electronic switches," *Nature*, vol. 479, no. 7373, pp. 329–37, Nov. 2011.
[3] S. Mookerjea, D. Mohata, R. Krishnan, J. Singh, A. Vallett, A. Ali, *et al.*, "Experimental demonstration of 100 nm channel length $In_{0.53}Ga_{0.47}As$-based vertical inter-band tunnel field effect transistors (TFET) for ultra low-power logic and SRAM applications," in *Proc. IEEE IEDM*, Dec. 2009, pp. 137.1–137.4.
[4] B. Radisavljevic, A. Radenovic, J. Brivio, V. Giacometti, and A. Kis, "Single-layer MoS_2 transistors," *Nat. Nanotechnol.*, vol. 6, no. 3, pp. 147–50, Mar. 2011.
[5] B. Radisavljevic, M. B. Whitwick, and A. Kis, "Integrated circuits and logic operations based on single-layer MoS_2," *ACS Nanotechnol.*, vol. 5, no. 12, pp. 9934–9938, Dec. 2011.

[6] Y. Yoon, K. Ganapathi, and S. Salahuddin, "How good can monolayer MoS_2 transistors be?" *Nano lett.*, vol. 11, no. 9, pp. 3768–3773, Sep. 2011.
[7] K. Kaasbjerg, K. S. Thygesen, and K. W. Jacobsen, "Phonon-limited mobility in n-type single-layer MoS_2 from first principles," *Phys. Rev. B*, vol. 85, no. 11, pp. 115317(1)–115317(16), Mar. 2012.
[8] A. Kuc, N. Zibouche, and T. Heine, "Influence of quantum confinement on the electronic structure of the transition metal sulfide TS_2," *Phys. Rev. B*, vol. 83, no. 24, pp. 245213(1)–245213(4), Jun. 2011.
[9] A. Kumar and P. K. Ahluwalia, "Electronic structure of transition metal dichalcogenides monolayers 1H-MX_2 (M = Mo, W; X = S, Se, Te) from ab-initio theory: New direct band gap semiconductors," *Eur. Phys. J. B*, vol. 85, no. 6, pp. 186(1)–186(9), Jun. 2012.
[10] K. Mak, C. Lee, J. Hone, J. Shan, and T. Heinz,"Atomically thin MoS_2: A new direct-gap semiconductor," *Phys. Rev. Lett.*, vol. 105, pp. 136805(1)–136805(4), Sep. 2010.
[11] S. Tongay, J. Zhou, C. Ataca, K. Lo, T. S. Matthews, J. Li, *et al.*, "Thermally driven crossover from indirect toward direct bandgap in 2D semiconductors: $MoSe_2$ versus MoS_2," *Nano Lett.*, vol. 12, pp. 5576–5580 Oct. 2012.
[12] S. H. El-Mahalawy and B. L. Evans, "Temperature dependence of the electrical conductivity and hall coefficient in 2H-MoS_2, $MoSe_2$, WSe_2, and $MoTe_2$," *Phys. Status Solid. B*, vol. 79, no. 2, pp. 713–722, Feb. 1977.
[13] H. R. Gutierrez, N. P. Lopez, A. L. Elias, A. Berkdemir, B. Wang, R. Lv, *et al.*, "Extraordinary room-temperature photoluminescence in triangular WS_2 monolayers," *Nano Lett.*, vol. 13, no. 8, pp. 3447–3454, Nov. 2012.
[14] G. H. Yousefi, "Optical properties of mixed transition metal dichalcogenide crystals," *Mater. Lett.*, vol. 9, no. 1, pp. 38–40, Dec. 1989.
[15] A. Splendiani, L. Sun, Y. Zhang, T. Li, J. Kim, C.-Y. Chim, *et al.*, "Emerging photoluminescence in monolayer MoS_2," *Nano Lett.*, vol. 10, pp. 1271–1275, Mar. 2010.
[16] A. C. -Gomez, N. Agraít, and G. R. -Bollinger, "Optical identification of atomically thin dichalcogenide crystals," *Appl. Phys. Lett.*, vol. 96, no. 21, pp. 213116(1)–213116(2), 2010.
[17] *QuantumWise Simulator*, Atomistix ToolKit (ATK) [Online]. Available: http://www.quantumwise.com/
[18] P. Pulay, "Convergence acceleration of iterative sequences the case of scf iteration," *Chem. Phys. Lett.*, vol. 73, no. 2, pp. 393–398, Jul. 1980.
[19] W. A. Harrison, *Solid State Theory*. New York, NY, USA: McGraw-Hill, 1970.
[20] R. M. Martin, *Electronic Structure*. Cambridge, U.K.: Cambridge Univ. Press, 2004.
[21] R. K. Ghosh and S. Mahapatra, "Direct band-to-band tunneling in reverse biased MoS_2 nanoribbon p-n junctions," *IEEE Trans. Electron Devices*, vol. 60, no. 1, pp. 274–279, Jan. 2013.
[22] R. K. Ghosh and S. Mahapatra, "Proposal for graphene-boron nitride heterobilayer based tunnel FET," *IEEE Trans. Nanotechnol.*, vol. 12, no. 5, pp. 665–667, Sep. 2013.
[23] M. Luisier and G. Klimeck, "Simulation of nanowire tunneling transistors: From the Wentzel-Kramers-Brillouin approximation to full-band phonon-assisted tunneling," *J. Appl. Phys.*, vol. 107, pp. 084507, Apr. 2010.
[24] R. K. Pandey, K. V. R. M. Murali, S. S. Furkay, P. J. Oldiges, and E. J. Nowak, "Crystallographic-orientation-dependent gate-induced drain leakage in nanoscale MOSFETs," *IEEE Trans. Electron Devices*, vol. 57, no. 9, pp. 2098–2105, Sep. 2010.
[25] S. M. Sze and K. K. Ng, *Physics of Semiconductor Devices*, 3rd ed. Hoboken, NJ, USA: Wiley, 2007.
[26] X. Guan, D. Kim, K. C. Saraswat, and H.-S. P. Wong, "Complex band structures: From parabolic to elliptic approximation," *IEEE Electron Device Lett.*, vol. 32, no. 9, pp. 1296–1298, Sep. 2011.
[27] M. A. Khayer and R. K. Lake, "Performance analysis of InP nanowire band-to-band tunneling field-effect transistors," *Appl. Phys. Lett.*, vol. 95, no. 7, pp. 073504(1)–073504(3), 2009.
[28] Z. Y. Zhu, Y. C. Cheng, and U. Schwingenschlogl, "Giant spin-orbit-induced spin splitting in two-dimensional transition-metal dichalcogenide semiconductors," *Phys. Rev. B*, vol. 84, no. 15, pp. 153402(1)–153402(5), Oct. 2011.
[29] K. Suzuki, T. Tanaka, Y. Tosaka, H. Horie, and Y. Arimoto, "Scaling theory for double-gate SOI MOSFET's," *IEEE Trans. Electron Devices*, vol. 40, no. 12, pp. 2326–2329, Dec. 1993.
[30] N. Patel, A. Ramesha, and S. Mahapatra, "Drive current boosting of n-type tunnel FET with strained SiGe layer at source," *Microelectron. J.*, vol. 39, no. 12, pp. 1671–1677, Dec. 2008.
[31] J. Appenzeller, J. Knoch, and M. T. Björk, "Toward nanowire electronics," *IEEE Trans. Electron Devices*, vol. 55, no. 11, pp. 2827–2845, Nov. 2008.
[32] D. Jena, "Tunneling transistors based on graphene and 2-D crystals," *Proc. IEEE*, vol. 101, no. 7, pp. 1585–1602, Jul. 2013.
[33] W. Y. Choi, B.-G Park, J. D. Lee, and T.-J. K. Liu, "Tunneling field-effect transistors (TFETs) with subthreshold swing (SS) less than 60 mV/dec," *IEEE Electron Device Lett.*, vol. 28, no. 8, pp. 743–745, Aug. 2007.
[34] Q. Zhang, T. Fang, H. Xing, A. Seabaugh, and D. Jena, "Graphene nanoribbon tunnel transistors," *IEEE Electron Device Lett.*, vol. 29, no. 12, pp. 1344–1346, Dec. 2008.
[35] *International Technology Roadmap for Semiconductors*, (2009) [Online]. Available: http://www.itrs.net/Links/2009ITRS/2009Chapters_2009Tables/2009_ExecSum.pdf
[36] Y. Sun, S. E. Thompson, and T. Nishida, *Strain Effect in Semiconductors: Theory and Device Applications*. New York, NY, USA: Springer-Verlag, 2010.
[37] T. Li, "Ideal strength and phonon instability in single-layer MoS_2," *Phys. Rev. B*, vol. 85, no. 85, pp. 235407(1)–235407(5), Jun. 2012.
[38] W. S. Yun, S. W. Han, S. C. Hong, I. G. Kim, and J. D. Lee, "Thickness and strain effects on electronic structures of transition metal dichalcogenides: 2H-MX_2 semiconductors (M = Mo, W; X = S, Se, Te)," *Phys. Rev. B*, vol. 85, no. 3, pp. 033305(1)–033305(5), Jan. 2012.
[39] K. H. Kao, A. S. Verhulst, W. G. Vandenberghe, B. Soree, G. Groeseneken, and K. D. Meyer, "Direct and indirect band-to-band tunneling in germanium-based TFETs," *IEEE Trans. Electron Devices*, vol. 59, no. 2, pp. 292–301, Feb. 2012.

Ram Krishna Ghosh received the M.Sc. degree in physics from the Indian Institute of Technology Madras, Chennai, India, in 2008, and the Ph.D. degree from the Department of Electronic Systems Engineering, Indian Institute of Science, Bangalore, India, in 2013. For the Ph.D dissertation, he focused on the exploration of real and complex dispersion relationship of nanomaterials for next generation transistor applications.

His current research interests include the ab-inito simulation-based quantum transport in nanoscale semiconductor devices for low power high speed applications.

Santanu Mahapatra (M'08–SM'10) received the B.E. degree from Jadavpur University, Kolkata, India, in the field of electronics and telecommunication, in 1999, the M. Tech degree in the field of electrical engineering (specializing in microelectronics) from the Indian Institute of Technology Kanpur, Kanpur, India, in 2001, and the Ph.D. degree from the Swiss Federal Institute of Technology, Lausanne, Switzerland, in 2005. For the Ph.D. dissertation, he focused on the modeling of single electron transistors and its cosimulation and codesign with CMOS.

He joined the Department of Electronic Systems Engineering, Indian Institute of Science (IISc), Bangalore, India, as an Assistant Professor in 2005, and then, was promoted to Associate Professor in 2010 on an out-of-the-term basis. He founded Nano Scale Device Research Laboratory in 2006, where his research team works on different areas of computational nanoelectronics. He has authored over 50 papers in SCI journals and graduated five Ph.D. students. He is the co-author of the book entitled *Hybrid CMOS Single Electron Transistor Device and Circuit Design* (Artech House, 2006). His current research interests include 2-D materials, ab-initio simulation, thermoelectric, compact modeling, and CMOS-nano hybridization.

Dr. Mahapatra was a recipient of the IBM Faculty award in 2007, the Microsoft Research India Outstanding Faculty Award in 2007, and the Associateship of Indian Academy of Sciences in 2009. He is also the first time recipient of the Ramanna Fellowship 2012 in the discipline of electrical sciences from the Department of Science and Technology, Government of India.